$Na_3Fe(CN)_5L{\cdot}nH_2O$ (where L = NH_3, ethylenediamine, pyridine, etc.) in the solid state.[28] In these cases, the endothermic peak associated with the removal of L was immediately followed by a slight exothermic peak, associated with a reorganization of primary products, i.e. $Fe(CN)_5^{3-}$, to $Fe(CN)_6Na_4$ and $Fe(CN)_6Fe_2$; the stoichiometry was effectively the same as in the aqueous system.

It is clear that a significant slow reduction of reactant concentration should occur in aqueous solutions of $Fe(CN)_5H_2O^{3-}$. On the other hand, it has been pointed out that the measurement of rates of substitution of water in $Fe(CN)_5H_2O^{3-}$ by various ligands presents serious difficulties unless oxygen is excluded from the medium.[1] Even in this case, however, kinetic complications still show up as slow absorbance changes, which are claimed to arise from the dissociation of dimers generated from $Fe(CN)_5H_2O^{3-}$.[29] We think that the presence of dimers at the dilution level usually employed (10^{-5} M) should be insignificant, as suggested by available data on the monomer–dimer equilibrium.[30] As shown in this work, $Fe(CN)_6^{4-}$ is likely to be present in the system because of the decomposition reaction, and this species may react with the added $Fe(CN)_5^{3-}$ scavenger through slow cyanide release.

Acknowledgment. The authors acknowledge the Comisiôn de Investigaciones Cientificas Prov. Bs. As. for partial financial support and to Dr. M. A. Blesa for valuable discussions.

Registry No. $Fe(CN)_5NH_3^{3-}$, 18497-51-3.

---

[28] (a) Gentil, L. A.; Olabe, J. A.; Baran, E. J.; Aymonino, P. J. *J. Therm. Anal.* **1975**, *7*, 279. (b) Olabe, J. A.; Gentil, L. A.; Baran, E. J.; Aymonino, P. J. *Monatsh. Chem.* **1975**, *106*, 941. (c) Morando, P. J.; Blesa, M. A. *Thermochim. Acta*, in press.

[29] Jwo, J. J.; Haim, A. *J. Am. Chem. Soc.* **1976**, *98*, 1172.

[30] Emschwiller, G. *C. R. Hebd. Seances Acad. Sci.* **1964**, *259*, 4281.

Contribution from the Chemistry Departments, Free University,
De Boelelaan 1083, 1081 HV Amsterdam, The Netherlands,
and University of Amsterdam, Nieuwe Achtergracht 166,
1018 WV Amsterdam, The Netherlands

Fe–Fe π Bonding in $Fe_2(CO)_6S_2$?

Roger L. DeKock,*[1a,b] Evert Jan Baerends,[1a] and Ad Oskam*[1c]

Received April 20, 1983

Currently, dinuclear transition-metal complexes are the subject of numerous investigations. In particular, data from ultraviolet photoelectron spectroscopy (UPS) and molecular orbital (MO) calculations provide a foundation for understanding the electronic structure of these types of complexes.

Recent studies on $Fe_2(CO)_6S_2$ include the UPS measurements and self-consistent field–Xα–scattered wave (SCF–Xα–SW) of Andersen et al.[2] and the He I/He II UPS and minimal basis ab initio calculations of van Dam et al.[3] The general empirical assignment of the photoelectron (PE) bands made in both papers is essentially identical. However, the theoretical description of the metal–metal bonding interaction in the two studies is different. The ab initio calculation describes the Fe–Fe interaction in terms of a single "bent" a_1-bonding (highest occupied) MO, in agreement with earlier Fenske–Hall calculations on the same molecule.[4] In the Xα–SW scheme a "bent" Fe–Fe bond was also calculated as the HOMO, but at about 2 eV more stable in energy a b_1 orbital[5] is calculated to have a significant direct Fe–Fe π component induced by the interaction with the bridging sulfur ligand. In view of the disagreement between the two calculated methods and the relatively poor agreement between the calculated and experimental ionization potentials (IP's), we have carried out Hartree–Fock–Slater (HFS) calculations on $Fe_2(CO)_6S_2$ using a double-ζ basis set. Numerous previous studies employing the HFS method have shown it to give excellent results in comparison to UPS measurements.[6] Our intent is both to examine the nature of the Fe–Fe bonding and to compare computed and experimental IP's.

Table I. Calculated and Experimental Results for $Fe_2(CO)_6S_2$

IP,[a] eV					Fe–Fe Mulliken
exptl	calcd	orbital level	% Fe 3d	% S	overlap population
		Band 1			
8.2 (sh)	8.14	$15a_1$	57	3	0.131
8.5 (sh)	8.49	$14a_1$	56	8	0.038
8.6	9.05	$13a_1$	69	9	0.022
	8.85	$8a_2$	80	0	−0.070
9.2 (sh)	8.54	$12b_2$	76	0	−0.073
	9.16	$11b_2$	75	2	−0.026
	8.57	$9b_1$	54	18	0.024
		Band 2			
10.2	10.16	$7a_2$	15	62	−0.013
10.8 (sh)	10.87	$8b_1$	40	49	0.040
		Band 3			
	12.46	$12a_1$	6	73	0.022
12.4	12.71	$11a_1$	16	68	0.039
	12.13	$10b_2$	9	61	−0.015

[a] sh = shoulder.

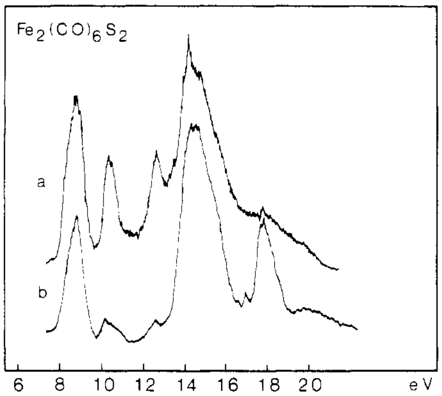

Figure 1. UV PE spectra of $Fe_2(CO)_6S_2$: a, He I spectrum; b, He II spectrum.

We present pertinent results in Table I. In computing the IP's we have employed the transition-state method for the same four transition states calculated by Andersen et al. For the other states we have employed an average of the calculated eigenvalues resulting from the four transition-state calculations. This procedure is justified since the eigenvalue shifts in each of the transition-state calculations is constant to within a few

---

[1] (a) Free University. (b) Address correspondence to Department of Chemistry, Calvin College, Grand Rapids, MI 49506. (c) University of Amsterdam.

[2] Andersen, E. L.; Fehlner, T. P.; Foti, A. E.; Salahub, D. R. *J. Am. Chem. Soc.* **1980**, *102*, 7422. Andersen's name was misspelled in the heading of this reference. The correct spelling is employed here.

[3] van Dam, H.; Louwen, J. N.; Oskam, A.; Doran, N.; Hillier, I. H. *J. Electron. Spectrosc. Relat. Phenom.* **1980**, *21*, 57.

[4] Teo, B. K.; Hall, M. B.; Fenske, R. F.; Dahl, L. F. *Inorg. Chem.* **1975**, *14*, 3103.

[5] *x*, *y*, and *z* axes are chosen as in ref 2; b_1 in this paper and in ref 2 corresponds to b_2 in ref 3.

[6] Baerends, E. J.; Ros, P. *Int. J. Quantum Chem.* **1978**, *12S*, 169. Heijser, W.; Baerends, E. J.; Ros, P. *Faraday Discuss. Chem. Soc.* **1980**, *No. 14*, 211. Jonkers, G.; De Lange, C. A.; Noodleman, L.; Baerends, E. J. *Mol. Phys.* **1982**, *46*, 609.

Table II. Percent Character of $8b_1$ Orbital from Different Calculational Methods

	Fe 3d	S		Fe 3d	S
Fenske-Hall[a]	38	48	HFS[c]	40	49
ab initio[b]	16	80	Xα-SW[d]	53	25

[a] Reference 4. [b] Reference 3. [c] This work. [d] Reference 2.

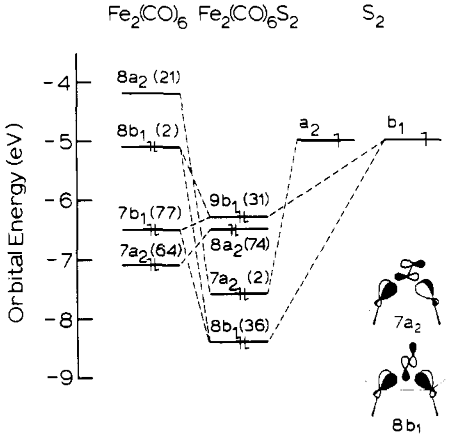

Figure 2. Energy-level diagram for the occupied π frontier orbitals of $Fe_2(CO)_6S_2$. The numbers next to each orbital refer to the percent d_π character in that orbital.

tenths of 1 eV. Notice the excellent agreement between experimental and computed IP's, which is typical for the HFS method. The computed IP's serve to confirm the assignment of the PE spectrum in the earlier publications.

Also in Table I we present the calculated percent character for each of the high-lying occupied valence MO's. The Fe 4s orbital contributes negligibly to these MO's, and the 4p orbital contribution varies between 0–7% so we have elected to report the Fe 3d character only. The orbitals assigned to band 1 in the PE spectrum are predominantly Fe 3d, those in band 2 ($7a_2$, $8b_1$) are a fairly strong mixture of Fe 3d and S character, and those in band 3 are predominantly S. The relative intensity changes in the He I/He II spectra (Figure 1) can be interpreted in terms of the Gelius model.[7] Upon going from He I to He II, PE bands assigned to Fe 3d character should increase in relative intensity whereas those assigned to S should decrease extremely.[8] Such is indeed the case in comparing the calculational and the experimental results.

In general there is relatively good agreement between the three sets of calculations regarding the percent character of the orbitals. However, the $8b_1$ orbital is calculated to have quite different character as seen in Table II.[9] This orbital is predominantly S in the ab initio calculation, but a strong mixture of Fe 3d/S in the other calculations. Close examination of the band shape change for band 2 upon going from He I to He II does support the contention that there is considerable metal character in the orbital ionized at about 10.8 eV (shoulder of band 2). Our orbital contour diagrams for the $8b_1$ orbital are essentially identical with those of Andersen et al.;[2] this indicates that the differing percent character of the $8b_1$ orbital presented in Table II is probably a matter of how the computational results are analyzed and not an essential difference in the calculated wave function (Xα–SW vs. HFS). The projected Xα–SW method of Bursten and Fenske[10] may serve to clarify the nature of the bonding in the case of Xα–SW calculations.

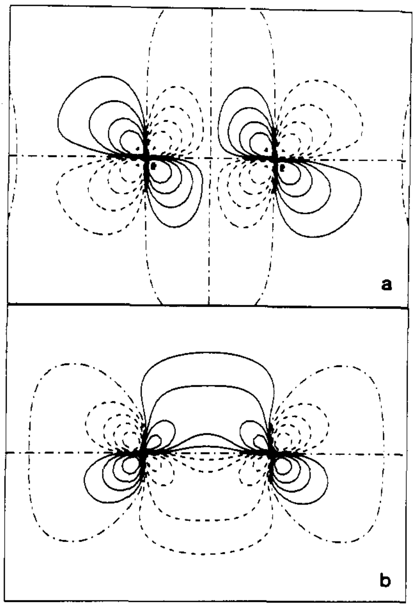

Figure 3. Computed orbital contour diagrams of $Fe_2(CO)_6S_2$: a, $8a_2$ orbital; b, $8b_1$ orbital. The contours are drawn in the *xy* plane where the *z* axis represents the twofold axis. The values of the contours are ±0.2, ±0.1, ±0.05, ±0.02, and the nodal contour.

With this background we now come to the question of Fe–Fe π bonding in $Fe_2(CO)_6S_2$. An orbital energy level diagram for the orbitals involved in Fe–Fe π bonding is presented in Figure 2. Also presented is the percent d_π character (b_1) and d_{π^*} character (a_2) for each orbital in the $Fe_2(CO)_6$ fragment and $Fe_2(CO)_6S_2$ molecule. The $7a_2$ and $7b_1$ MO's of $Fe_2(CO)_6$ belong to what is nominally referred to as the $(t_{2g})^6$ "nonbonding" orbitals.[11] The $7a_2$ MO of $Fe_2(CO)_6$ correlates strongly with $8a_2$ of $Fe_2(CO)_6S_2$. Therefore, in the a_2 representation (Fe–Fe π*) the $8a_2$ MO of $Fe_2(CO)_6S_2$ correlates only with $7a_2$ of $Fe_2(CO)_6$ and a_2 of S_2. However, in the b_1 representation (Fe–Fe π) there is a strong mixing together of $7b_1$ and $8b_1$ of $Fe_2(CO)_6$ with b_1 of S_2 to form $8b_1$ and $9b_1$ of $Fe_2(CO)_6S_2$. Notice that the 77% d_π character of $7b_1$ for $Fe_2(CO)_6$ is now "diluted" over 36% d_π in $8b_1$ of $Fe_2(CO)_6S_2$ and 31% d_π in the $9b_1$ MO. We agree with Andersen et al. that the $8b_1$ MO does represent an Fe–Fe π-bonding orbital, but it has been achieved at the expense of Fe–Fe π bonding in the $9b_1$ orbital. The π bonding of $8b_1$ and $9b_1$ are canceled by the π* antibonding of $8a_2$. This analysis is borne out by the orbital contour diagrams for the $8b_1$ and $8a_2$ MO's (Figure 3).

In summary, our results indicate that the total analysis of the Fe–Fe π bonding must take into account not only the relevant Fe–S interaction orbitals ($7a_2$, $8b_1$) but also the corresponding orbitals ($8a_2$, $9b_1$) from the $(t_{2g})^6$ "nonbonding" set. Consequently, the Fe–Fe bond is best described in terms of a single "bent" a_1-bonding orbital, namely the HOMO ($15a_1$).

Acknowledgment. This work was supported in part by financial aid from the Netherlands Organization for the Advancement of Pure Research (ZWO). R.D.K. also acknowledges the grant support of the Netherlands America Commission for Educational Exchange and of Calvin College for a Calvin Research Fellowship.

Registry No. Fe, 7439-89-6; $Fe_2(CO)_6S_2$, 58500-79-1.

---

(7) Berndtsson, A.; Basiliev, E.; Gelius, U.; Klasson, M.; Nilsson, R.; Nordling, C.; Svenson, S. *Phys. Scr.* **1975**, *12*, 235.

(8) Schweig, A.; Thiel, W. *J. Chem. Phys.* **1974**, *60*, 951.

(9) The $8b_1$ orbital is comprised of the π* S_2 orbital and appropriate b_1 fragment orbitals of $Fe_2(CO)_6$. Similar differences in percent character are observed in the other component of the π* S_2 orbital interacting with the $Fe_2(CO)_6$ orbitals in the a_2 representation ($7a_2$). In each case the $7a_2$ orbital is mainly sulfur, but its sulfur contribution varies between 39% and 86% depending upon the method of calculation.

(10) Bursten, B. E.; Fenske, R. F. *J. Chem. Phys.* **1977**, *67*, 3138. Bursten, B. E.; Freier, D. G.; Fenske, R. F. *Inorg. Chem.* **1980**, *19*, 1811.

(11) Thorn, D. L.; Hoffmann, R. *Inorg. Chem.* **1978**, *17*, 126.